ENHANCED FORCE CALCULATION FOR AXISYMMETRIC FINITE ELEMENT MODELS

Herbert De Gersem Kay Hameyer
Katholieke Universiteit Leuven, Dep. EE (ESAT), Div. ELEN
Kardinaal Mercierlaan 94, B-3001 Leuven, Belgium
E-mail: Herbert.DeGersem@esat.kuleuven.ac.be

Abstract - The force computed by the classical Maxwell stress method along a contour between two bodies in a finite element model, depends on the chosen contour of integration and the local orientation of the mesh. The numerical differentiation of the discrete solution for the magnetic vector potential leads to the loss of one order of the convergence rate. An enhanced force calculation approach for axisymmetric models is proposed. A series solution consisting of analytical terms is constructed in the region between the moving bodies. The Maxwell stress method is applied to the local analytical solution. The method is used to compute a tubular permanent magnet synchronous machine. An improved convergence of the force error at decreasing mesh sizes can be stated.

1. Introduction

In numerical simulations, a trade-off is made between the desired accuracy of the results and the numerical problem size. The discretization error of finite element calculation is controlled by choosing an appropriate fine mesh. The force computation introduces a significant loss of accuracy when compared to the potential solution. An increased problem size may disable the possibility of numerical design and optimization for technical devices. In this paper, an enhanced force computation technique is developed to keep the error propagation as small as possible. An effective balance between accuracy and simulation speed is obtained by using first order finite elements combined with a mesh adaptation algorithm. Severe refinement of the model is avoiding by using highly accurate post-processing and force computation.

2. Axisymmetric magnetostatic formulation

The divergence-free condition for the magnetic flux density $\mathbf{B}$ is imposed by the relation $\mathbf{B} = \nabla \times \mathbf{A}$ where $\mathbf{A}$ denotes the magnetic vector potential. In the magnetostatic case, Ampère's law leads to the elliptic partial differential equation

$$\nabla \times \left(\nu \nabla \times \mathbf{A} \right) = \mathbf{J} \,, \tag{1}$$

where ν is the magnetic permeability and $\mathbf{J}$ the imposed current density. In a model with a cylindrical geometry, cylindrical boundary conditions and excited by currents J_θ in the tangential θ-direction, the magnetic field appears only in the (r,z)-plane. The magnetic vector potential has only a tangential component A_θ. Therefore, Equ. 1 is reduced to[1]

$$\frac{\partial}{\partial r}\left(\frac{\nu}{r} \frac{\partial \left(r A_\theta \right)}{\partial r} \right) + \frac{\partial}{\partial z}\left(\nu \frac{\partial A_\theta}{\partial z} \right) = -J_\theta \,. \tag{2}$$

The axisymmetric domain is discretized by the triangular first order finite elements N_j:

$$A_\theta = \sum_j A_{\theta j} N_j \,. \tag{3}$$

3. Force computation based on the Maxwell stress tensor

The magnetic flux density in an axisymmetric model,

$$\mathbf{B} = \left(B_r, 0, B_z \right) = \left(-\frac{\partial A_\theta}{\partial z}, 0, \frac{1}{r} \frac{\partial \left(r A_\theta \right)}{\partial r} \right), \tag{4}$$

is derived out of the finite element solution by a numerical post-processing step. The partial differentiations operate on the form functions:

$$\mathbf{B} = \sum_j A_{\theta j} \left(-\frac{\partial N_j}{\partial z}, 0, \frac{\partial N_j}{\partial r} + \frac{1}{r} N_j \right). \tag{5}$$

The r-component of the flux density is piecewize constant whereas the z-component is built of a constant and a hyperbolic term (Fig. 1b). The flux density is less accurate than the linear approximated potential solution[2] (Fig. 1a).

In axisymmetric models, the force components in the θ-direction and the r-direction vanish. The force equals the integral of the Maxwell stress tensor in the z-direction $\mathbf{T}_z$ along a contour C, around the moving body:

$$F_z = \oint_C 2\pi r \nu \mathbf{T}_z \cdot \mathrm{d}\,\ell = \oint_C 2\pi r \nu \left(B_r B_z, 0, \frac{B_z^2 - B_r^2}{2} \right) \cdot \mathrm{d}\,\ell \,. \tag{6}$$

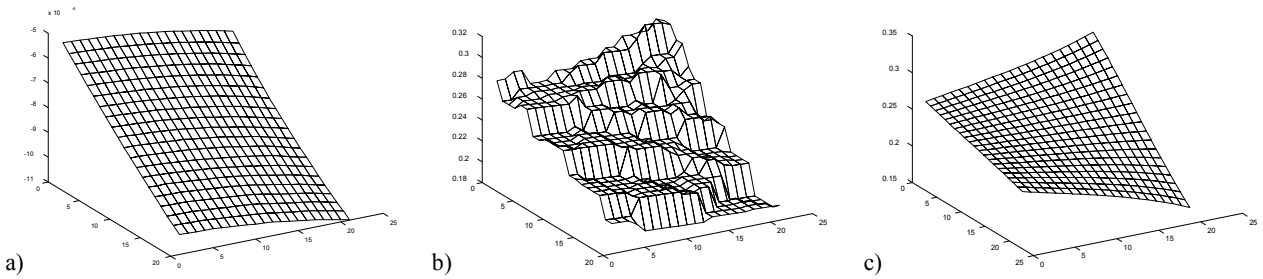

a) b) c)

Fig. 1 a) Finite element solution A_θ, b) B_r obtained numerically and c) B_r obtained by local analytic post-processing.

In a tubular device, the force is computed along a line in the air gap and parallel to the axis of symmetry:

$$F_z = \int_{z_1}^{z_2} \nu_0 B_r B_z \, 2\pi r \, dz \, . \tag{7}$$

The force integral relies on the flux densities. Moreover, a discrete integration along an arbitrary contour through the discontinuous flux density distribution causes a harmfull error propagation in the force computation.

4. Discretization error

The quality of a finite element simulation is measured in terms of the global error ε on the solution. An a priori estimate is

$$\|\varepsilon\| \le C \cdot h^p \, , \tag{8}$$

where h is the characteristic mesh size, p the asymptotic rate of convergence and C the convergence factor[3]. The convergence rate expresses the exponential decay of the discretization error according to the decreasing mesh size h. The convergence factor is an upper bound independent of the mesh size and is influenced by the aspect ratio of the elements, the accuracy of the numerical integration and rounding-off errors.

The asymptotic rate of convergence of the finite element solution is related to the nature of the partial differential equation and the choice of base and test functions. In the case of elliptic partial differential equations discretized by polynomial finite elements, the error decays as

$$\|\varepsilon\| \le C \cdot h^{q+1} \, , \tag{9}$$

where q denotes the polynomial order of the elements[2-3]. Using first order elements, the rate of convergence for the magnetic vector potential is $O(h^2)$. Equivalently, in terms of the number of degrees of freedom (DOF), the convergence of axisymmetric solutions is of order $O(DOF^{-1})$.

The global error of derived field information depends on the discretization error on the potential solution and the error propagation in the post-processing routines. Additions and multiplications only alter the convergence factor. Numerical differentiation, however, introduces the loss of one order of the asymptotic convergence rate. Flux densities, reluctivities and forces obtained by differentiating the magnetic vector potential only exhibit a convergence of order $O(h^q)$. A sufficiently accurate potential field may bring up forces that do not reach the same prescribed limit. Moreover, increasing the accuracy of force calculation is obtained at the expense of exponential growing computational efforts.

5. Local analytic post-processing

To keep the same convergence rate as the finite element solution, the harmfull numerical differentiation in the force calculation scheme has to be avoided. This is possible if a representation for the potential solution is available in a form that is independent of the local discretization and is free from base functions suffering from numerical differentiation[4-5]. The Green's functions related to the partial differential equation form a function base allowing accurate differentiation. An analytical solution in terms of Green's functions is constructed in a homogeneous subdomain of the model, using the finite element solution as a boundary condition. The convergence rate equals that of the boundary condition. As the computation of derived quantities out of an analytic solution has no influence on the convergence rate of the error, a computation principle for highly accurate post-processing is developed. This approach is called *superconvergent* as it establishes a higher convergence rate for derived quantities than predicted by the finite element theory[2].

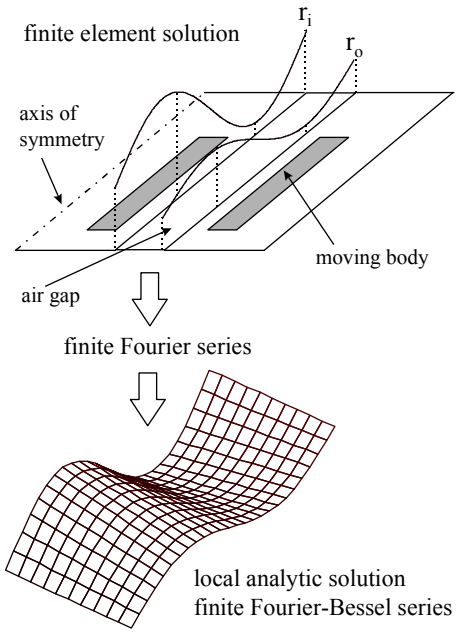

Fig. 2 Algorithm of the enhanced force calculation technique: finite element solution, finite Fourier series and local analytic solution.

6. Local analytic solution for an axisymmetric magnetic field

Consider a local post-processing domain between two moving bodies. The domain contains a homogeneous, isotropic and linear material. There are no imposed currents. The governing differential equation is

$$\frac{\partial}{\partial r}\left(\frac{1}{r}\frac{\partial (r A_\theta)}{\partial r}\right) + \frac{\partial^2 A_\theta}{\partial z^2} = 0 \, . \tag{10}$$

The analytic solution is a series in terms of the Green's functions associated with the partial differential equation:

$$\begin{aligned} A_\theta = \sum_k \big(&\alpha_k \cos(\lambda_k z) + \beta_k \sin(\lambda_k z)\big) \\ &\cdot \big(\chi_k \, \mathrm{I}_1(\lambda_k r) + \delta_k \, \mathrm{K}_1(\lambda_k r)\big) \\ &+ \big(\varepsilon_k \sinh(\lambda_k z) + \phi_k \cosh(\lambda_k z)\big) \\ &\cdot \big(\gamma_k \, \mathrm{J}_1(\lambda_k r) + \eta_k \, \mathrm{Y}_1(\lambda_k r)\big) \, , \end{aligned} \tag{11}$$

where α_k, β_k, χ_k, δ_k, ε_k, ϕ_k, γ_k and η_k are unknown coefficients, J_p and Y_p are Bessel functions of order p and I_p and K_p are modified Bessel functions of order p[6].

The finite element solution serves as the boundary conditions for the local partial differential problem. The

magnetic vector potential values are extracted out of the finite element solution at the inner and outer boundaries, $r = r_i$ and $r = r_o$, of the subdomain and are represented by the n-points Fourier transforms

$$A_\theta(r_i,z) = \sum_{k=0}^{n}\left(a_{k,i}\cos(\lambda_k z) + b_{k,i}\sin(\lambda_k z)\right) \tag{12}$$

and

$$A_\theta(r_o,z) = \sum_{k=0}^{n}\left(a_{k,o}\cos(\lambda_k z) + b_{k,o}\sin(\lambda_k z)\right). \tag{13}$$

The periodicity of the model in the z-direction,

$$A_\theta(r,z+\ell_z) = A_\theta(r,z), \tag{14}$$

causes the hyperbolic terms in Equ. 11 to disappear. The set of possible spatial frequencies λ is then

$$\left\{\lambda \,\middle|\, \lambda = \frac{2\pi k}{\ell_z},\ k \in /N\right\}. \tag{15}$$

The local analytic solution for the periodic axisymmetric magnetostatic field problem is the Fourier-Bessel series

$$A_\theta = \sum_{k=0}^{\infty}\left(a_k\cos(\lambda_k z)\,\mathrm{I}_1(\lambda_k r) + b_k\sin(\lambda_k z)\,\mathrm{I}_1(\lambda_k r) + c_k\cos(\lambda_k z)\,\mathrm{K}_1(\lambda_k r) + d_k\sin(\lambda_k z)\,\mathrm{K}_1(\lambda_k r)\right), \tag{16}$$

where a_k, b_k, c_k and d_k still depend on the boundary conditions on $r = r_i$ and $r = r_o$.

An approximative local analytic solution is formed by the n-terms truncated version of Equ. 16 (Fig. 2). The coefficients a_k, b_k, c_k and d_k follow from

$$\begin{bmatrix}\mathrm{I}_1(\lambda_k r_i) & \mathrm{K}_1(\lambda_k r_i)\\ \mathrm{I}_1(\lambda_k r_o) & \mathrm{K}_1(\lambda_k r_o)\end{bmatrix}\cdot\begin{bmatrix}a_k\\ c_k\end{bmatrix} = \begin{bmatrix}a_{k,i}\\ a_{k,o}\end{bmatrix},\ k = 1,\ldots,n \tag{17}$$

and

$$\begin{bmatrix}\mathrm{I}_1(\lambda_k r_i) & \mathrm{K}_1(\lambda_k r_i)\\ \mathrm{I}_1(\lambda_k r_o) & \mathrm{K}_1(\lambda_k r_o)\end{bmatrix}\cdot\begin{bmatrix}b_k\\ d_k\end{bmatrix} = \begin{bmatrix}b_{k,i}\\ b_{k,o}\end{bmatrix},\ k = 1,\ldots,n\,. \tag{18}$$

7. Force calculation based on the local analytic solution

The magnetic flux density inside the post-processing area is derived from Equ. 4 and Equ. 16 analytically.

$$B_r = \sum_{k=1}^{n}\lambda_k\left(a_k\sin(\lambda_k z)\,\mathrm{I}_1(\lambda_k r) - b_k\cos(\lambda_k z)\,\mathrm{I}_1(\lambda_k r) + c_k\sin(\lambda_k z)\,\mathrm{K}_1(\lambda_k r) - d_k\cos(\lambda_k z)\,\mathrm{K}_1(\lambda_k r)\right) \tag{19}$$

$$B_z = \sum_{k=1}^{n}\lambda_k\left(a_k\cos(\lambda_k z)\,\mathrm{I}_0(\lambda_k r) + b_k\sin(\lambda_k z)\,\mathrm{I}_0(\lambda_k r) - c_k\cos(\lambda_k z)\,\mathrm{K}_0(\lambda_k r) - d_k\sin(\lambda_k z)\,\mathrm{K}_0(\lambda_k r)\right) \tag{20}$$

The local analytic expressions for the flux density is less dependent on the local mesh and reaches almost the same accuracy as the finite element solution itself (Fig. 1c).

The force in the z-direction is analytically integrated along a line $r = r_m$ parallel to the axis and inside the analytic post-processing domain:

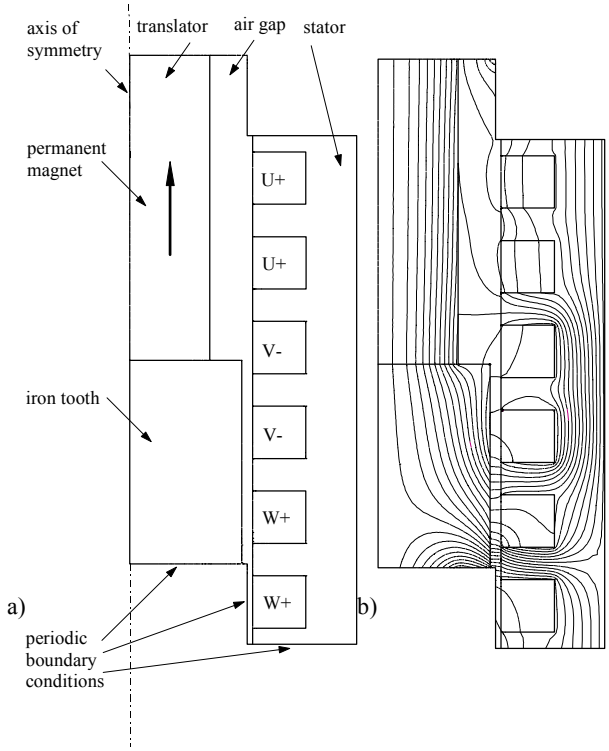

Fig. 3 (a) Geometry and (b) magnetic flux lines of the tubular permanent magnet synchronous machine.

$$F_z = 2\pi r_m\,\nu_0\,\frac{\ell_z}{2}\sum_{k=1}^{n}\left(\lambda_k^2\left(b_k c_k - a_k d_k\right)\cdot\left(\mathrm{I}_1(\lambda_k r_m)\,\mathrm{K}_0(\lambda_k r_m) + \mathrm{I}_0(\lambda_k r_m)\,\mathrm{K}_1(\lambda_k r_m)\right)\right). \tag{21}$$

The equality $\mathrm{I}_1(t)\,\mathrm{K}_0(t) + \mathrm{I}_0(t)\,\mathrm{K}_1(t) = \frac{1}{t}$ [6] is used to rearrange Equ. 21 to

$$F_z = 2\pi^2\,\nu_0\sum_{k=1}^{n}k\left(b_k c_k - a_k d_k\right). \tag{22}$$

The force does not depend on the actual chosen contour $r = r_m$. The fundamental difference and advantage to commonly used averaging techniques is that the force is directly obtained from the second order convergent potential field instead of from the first order convergent flux densities. A strong resemblance is seen between Equ. 22 and an analogue expression for the torque in 2D cartesian models[2].

8. Application

The three-phase stator winding of a four-pole tubular permanent magnet synchronous machine consists of two slots per pole and per phase[7] (Fig. 3a). The permanent magnets on the translator are magnetized in the z-direction. The active length of the air gap depends on the position of the translator. The symmetry of the geometry and the excitation allows the modelling of a single pole. Periodic boundary conditions connect the upper and lower boundaries. The computation is performed for different load angles and translator positions. The short-stator and short-rotor effects, characteristic for linear

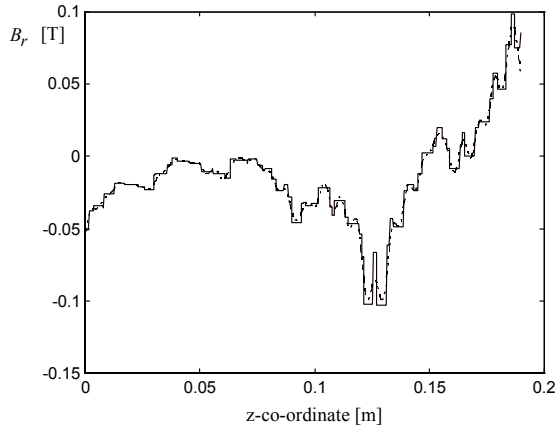

Fig. 4 Finite element solution (solid) and local post-processing solution (dotted) for B_r along a line in the middle of the air gap.

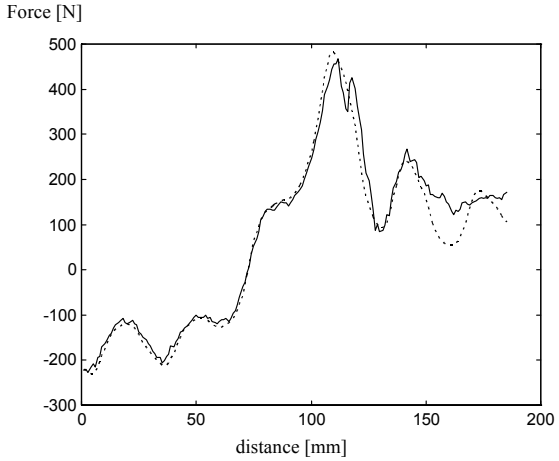

Fig. 5 Force in terms of the load angle computed on 1000 node meshes (solid) and on 10000 node meshes (dotted).

motors[8], are considered approximatively.

The first order finite element solution is shown in Fig. 3b. A rectangular domain in the middle of the air gap forms the local post-processing domain. The magnetic vector potentials of the finite element solution extracted along the inner and outer boundaries of the domain, are treated as 256-points finite Fourier series. A finite Fourier-Bessel series forms the analytical solution for the potential in the considered area. The magnetic flux densities obtained by the local analytic post-processing are compared to those obtained purely numerically (Fig. 4). The force for different load angles is plotted in Fig. 5.

Fig. 6 compares the convergence behaviours of the force errors of the classical Maxwell stress method and the enhanced force computation technique. The classical force computation scheme converges with the order $O(DOF^{-½})$ whereas the enhanced technique reaches $O(DOF^{-1})$. The economical-technical importance of the improved force computation is the fact that a certain accuracy (f.i. 0.5% in Fig. 6) is reached with a smaller finite element problem size (3000 DOFs instead of 10000 DOFs) or a desired accuracy for the force is attainable within the existing calculation resources (f.i. 0.1% in Fig. 6).

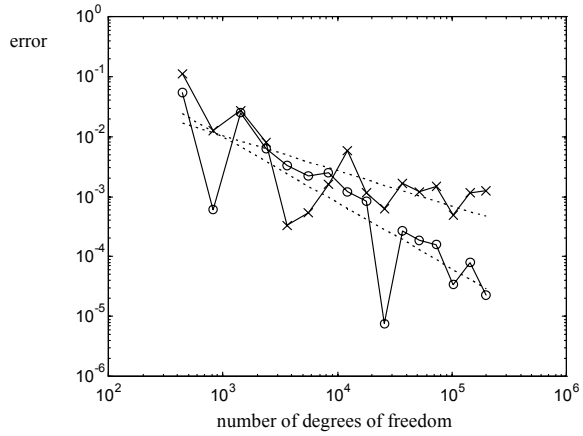

Fig. 6 Convergence of the Fourier-Bessel based (o) and classical (x) force computation methods.

9. Conclusion

The troublesome numerical differentiation of the magnetic vector potential while applying the Maxwell stress method for force calculation is avoided by constructing and using a local analytic solution in the air gap between the moving bodies of an actuator. A second order convergence is stated for the global force error in the simulation of a tubular permanent magnet synchronous machine. The convergence of the force error is the same as at the finite element solution. The enhanced approach makes a further mesh refinement or an increased element order superfluous.

Acknowledgement

The authors are grateful to the Belgian "Fonds voor Wetenschappelijk Onderzoek Vlaanderen" (project G.0427.98) for its financial support of this work and the Belgian Ministry of Scientific Research for granting the IUAP No. P4/20 on Coupled Problems in Electromagnetic Systems. The research Council of the K.U.Leuven supports the basic numerical research.

Reference

[1] P.P. Silvester and R.L. Ferrari, *Finite Elements for Electrical Engineers*, 3rd ed., Cambridge University Press, New York, 1996.

[2] K. Hameyer, R. Mertens, U. Pahner, R. Belmans, "New technique to enhance the accuracy of 2-D/3-D field quantities and forces obtained by standard finite-element solutions", *IEE Proc.-Sci. Meas. Technol.*, Vol. 145, No. 2, March 1998, pp. 67-75.

[3] C. Johnson, *Numerical Solution of Partial Differential Equations by the Finite Element Method*, Cambridge University Press, Cambridge, 1987.

[4] P.P. Silvester and D. Omeragic, "Differentiation of finite element solutions of the Poisson equation", *IEEE Trans. on Magnetics*, Vol. 29, No. 2, March 1993, pp. 1993-1996.

[5] M. Kasper and J. Franz, "Highly accurate computation of field quantities and forces by superconvergence in finite

elements", *IEEE Trans. on Magnetics*, Vol. 31, No. 3, May 1995, pp. 1424-1427.

[6] G.N. Watson, *A Treatise on the Theory of Bessel Functions*, Cambridge University Press, Cambridge, 1966.

[7] T.J.E. Miller, *Brushless Permanent-Magnet and Reluctance Motor Drives*, Clarendon Press, Oxford, 1989.

[8] E.R. Laithwaite, *Induction Machines for Special Purposes*, Newnes, London, 1966.